Proceedings of the 2005 IEEE
International Symposium on Intelligent Control
Limassol, Cyprus, June 27-29, 2005

Modeling and Control of a Shape Memory Alloy Actuator

Sushant M. Dutta, Fathi H. Ghorbel, and James B. Dabney

Abstract— **In this paper, we present a complete mathematical model of a spring-biased shape memory alloy (SMA) wire actuator driven by an electric current. The working of the SMA actuator is based on diverse physical phenomena, viz., heat convection, phase transformation, stress-strain variations and electrical resistance variation accompanying the phase transformation. The proposed model decomposes the operation of the actuator into these phenomena and comprises modules which represent each of these phenomena independently. The phase transformation involves significant temperature hysteresis. We model this hysteresis by a differential hysteresis model, which can conveniently represent both major and minor loops. We also propose a differential inverse of the hysteresis model, whereby, we obtain the differential inverse of the complete SMA actuator model. We propose a feedback control scheme with inverse compensation based on the inverse SMA model. Simulation results are presented, which demonstrate the effectiveness of the proposed control technique.**

KEYWORDS

Shape memory alloy, hysteresis, modeling, phase transformation, feedback control, inverse compensation.

I. INTRODUCTION

Shape memory alloys (SMAs) are metallic alloys which exhibit the shape memory effect, i.e., a SMA can be deformed at low temperature but regains its original undeformed configuration when heated to a higher temperature. This is due to the reversible crystalline phase transformation that occurs between the low temperature martensite (M) phase and the high temperature austenite (A) phase of the SMA. The two phases have very different thermal, mechanical and electrical properties, owing to their different crystallographic structures. In the absence of applied stress, the M phase is formed without any observable change of geometry. However, when an external stress is applied to the M phase, it causes a large inelastic strain in the SMA. When the SMA is heated to a higher temperature, the SMA reverts to the symmetric A phase via a phase transformation. This phase transformation is accompanied by a large force against the applied stress and recovery of the inelastic strain. The combination of large recovery strain, high strength, and high stiffness, makes SMAs ideal for use as actuators in a variety of applications. Typical examples can be found in [1], [2], [3], [4], [5], [6], [7], [8], [9]. In addition, it is easy to drive a SMA actuator by passing an electric current through it, which heats up the SMA via the Joule effect. Unfortunately, cooling cannot be similarly controlled, and one has to rely on natural air convection, or possibly coolant fluids, to cool the SMA. This places an inherent bound on the operating frequency of SMA actuators.

The $A - M$ phase transformation is a fundamental property of SMAs, and is characterized by the martensite fraction R_m, which is defined as the volume fraction of martensite present in the SMA at any instant. By definition, $R_m \in [0, 1]$. It is known that the $A - M$ phase transformation exhibits significant temperature hysteresis [10]. A schematic diagram of the typical hysteresis between martensite fraction and temperature is shown in Fig. 1. This phase transformation hysteresis is characterized by transformation temperatures; austenite start temperature A_s, austenite finish temperature A_f, martensite start temperature M_s, and martensite finish temperature M_f.

SMA wire is the most commonly used form of SMA actuator because of its ease of use and convenient electrical activation. A schematic diagram of a spring-biased SMA wire actuator is shown in Fig. 2. L_0 is the undeformed length of the SMA wire heated to 100% austenitic state and at zero pretension. ϵ_0 is the strain caused by spring pretension, while the SMA is still heated to 100% austenitic state. ϵ_r is the recoverable strain caused by $A - M$ phase transformation. The total strain is $\epsilon = \epsilon_0 + \epsilon_r$. We present a complete mathematical model of this spring-biased SMA wire actuator, and we propose a model-based tracking control scheme.

We use experimental results of Ma *et al.* [11] for modeling and identification. The construction and details of the experimental setup can be found in [11]. A potential difference $v(t)$ is applied across the SMA wire using a programmable power supply. This causes an electric current $i(t)$ to flow through the SMA wire, which gets heated up via the Joule effect. Both $v(t)$ and $i(t)$ are measurable in real-time. Therefore, power vi and electrical resistance $R = v/i$ can also be computed in real-time. The output variable is the transformation strain ϵ_r. The actual strain is measured using a Linear Variable Differential Transformer.

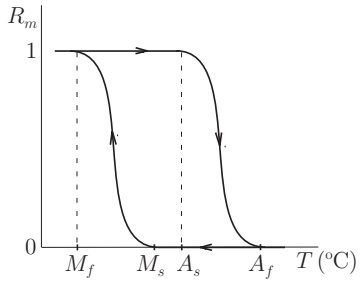

Fig. 1. Schematic of martensite fraction–temperature hysteresis

S.M. Dutta and F.H. Ghorbel are with the Department of Mechanical Engineering and Materials Science, Rice University, Houston, TX 77005 USA smdutta,ghorbel@rice.edu

J.B. Dabney is with the Department of Systems Engineering, University of Houston - Clear Lake, Houston, TX 77058 USA dabney@cl.uh.edu

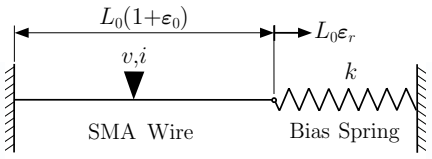

Fig. 2. Schematic of spring-biased SMA wire actuator

The motivation behind modeling of SMA wire actuator is to be able to control ϵ_r to follow a desired strain $\epsilon_{rd}(t)$. Thus, the SMA wire actuator system can be considered to be any one of the following I/O systems: (a) $v(t) - \epsilon_r(t)$, (b) $i(t) - \epsilon_r(t)$, (c) $R(t) - \epsilon_r(t)$ or (d) $vi - \epsilon_r(t)$. The system dynamics are shown in Fig. 3.

Position control strategies of SMA actuators can be divided into two broad categories. One method uses actual strain measurement and a feedback control loop, whereby the strain error is minimized using any of the several standard closed loop control schemes. However, strain measurement might be expensive [11] or impractical [12]. The other method is to use a mathematical model of the actuator, which predicts the actuator strain $\hat{\epsilon_r}$. This gives us two control options:

- feedback control using computed error $e = \epsilon_{rd} - \hat{\epsilon_r}$, and
- model-based control using inverse dynamics model.

Thus, mathematical modeling of SMA actuators is invaluable to developing control systems for them. Even though new applications for SMA actuators have abounded over the years, their mathematical modeling is still an open research problem. Ikuta *et al.* [10] proposed the *variable sublayer model* to derive expressions for both strain and electrical resistance of SMAs. The variable sublayer model hypothesizes that the SMA consists of parallel connected sublayers of different phases with different mechanical characteristics. They also proposed a phenomenological algebraic model for martensite fraction–temperature hysteresis. Their resistance modeling did not produce satisfactory results. It has also been shown [13] that the hysteresis model developed in [10] is not suitable for simulation of a closed-loop control system.

Brailovski *et al.* [14] used a lumped parameter convective heat transfer equation to generate the temperature profile for SMAs, given the voltage and the current. Madill and Wang [13] also used the same equation, assuming constant parameters. They extended the work of [10] to model a SMA wire actuator under constant load and used the model to propose an L2-stable position proportional control system. However, it has been shown that the parameters in the heat transfer equation are temperature-dependent [15], [16]. Recently, Ma *et al.* [11] modeled the system dynamics of Fig. 3 as a black box. They used a neural network model of $R(t) - \epsilon_r(t)$ for position PID control of a spring-biased SMA wire actuator. However, they did not model minor hysteresis loops.

An important part of SMA modeling is hysteresis modeling, and it has been studied extensively in the literature. Bo and Lagoudas [17] have compiled an exhaustive review of hysteresis modeling in SMAs. The Preisach model has been widely used to model SMA hysteresis. However, the computation of the weighting function for every point in the hysteresis region is a tedious process. Algebraic models for SMA hysteresis in the literature include [10], [13], [17], [18], [19]. From the point of view of control systems, a differential model of hysteresis has significant advantages. A differential model can conveniently form a state space system along with the SMA dynamics equations. Hence, the theory of ordinary differential equations can be used for analysis of the dynamic system. However, probably the only differential model of SMA hysteresis in the literature is one by Likhachev [20].

In this paper, we follow a modular approach to modeling each system element (see Fig. 3) of the spring-biased SMA wire actuator shown in Fig. 2. Our approach is illustrated in Fig. 4. Based on this model, we propose a tracking controller design that uses feedback with inverse compensation. Our main contributions are as follows:

1) We propose temperature-dependent parameters for the lumped parameter convective heat transfer equation to obtain accurate temperature profile. (Fig. 4, module *I*)
2) We propose special forms of functions for Likhachev's general differential hysteresis model [20] for modeling the major and minor hysteresis loops. (Fig. 4, module *II*)
3) We extend the variable sublayer model [10] and Madill and Wang's strain analysis [13] to the case of spring-biased SMA wire actuator. (Fig. 4, module *III*)
4) We propose nonlinear temperature coefficients of resistivity and use the variable sublayer model [10] to model SMA resistance. (Fig. 4, module *IV*)
5) We show that the proposed model is invertible. Using this property, we develop a tracking control system which is based on a combination of open loop feedforward inverse compensation and closed loop PD control.

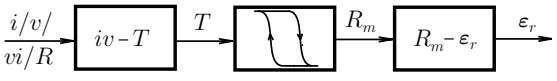

Fig. 3. Block diagram of SMA wire actuator system

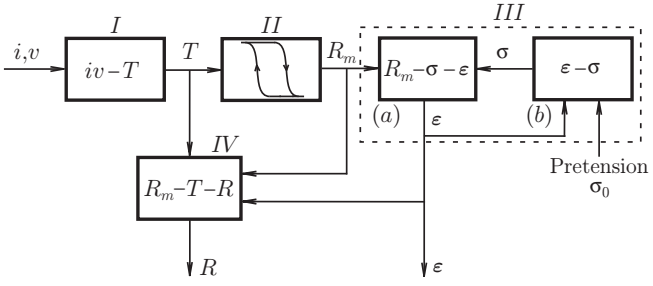

Fig. 4. Proposed differential model block diagram

The remainder of the paper is organized as follows. Section II presents the differential model for spring-biased SMA wire actuator. Section III presents the tracking control system based on model-based inverse compensation with PD feedback. Section IV discusses simulation results. In Section V, we present our conclusions.

II. Differential Modeling: Modular Approach

Our modeling strategy was illustrated in Fig. 4. Each physical process involved in the SMA operation is modeled separately. This section presents the differential model equations very briefly. The details are available in [21].

A. Joule Heating and Heat Transfer

Given the input electric power vi to the SMA wire, its temperature T is given by the heat transfer equation

$$\rho c \frac{\pi d_0^2 L_0}{4} \frac{dT}{dt} \approx vi - \pi d_0 L_0 h (T - T_{amb}) . \qquad (1)$$

where d_0 is the cross-sectional diameter of the undeformed wire, T_{amb} is the ambient temperature, ρ is the mass density of the wire, c is the specific heat of the wire, and h is the convective heat transfer coefficient of the wire. h and c are functions of temperature and are given by

$$h = \begin{cases} a_1 - a_2 T, & \dot{T} \geq 0, \\ a_3 + a_4 \operatorname{erf}\left(\frac{T-m_1}{n_1}\right), & \dot{T} < 0, \end{cases} \qquad (2)$$

$$c = b_1 + b_2 \operatorname{erf}\left(\frac{T-m_2}{n_2}\right), \qquad (3)$$

where a_1, a_2, a_3, a_4, b_1, b_2, m_1, n_1, m_2 and n_2 are constant parameters.

The equations in this section constitute part *I* of Fig. 4.

B. Phase Transformation Hysteresis

At the heart of the proposed SMA actuator model is the Duhem differential hysteresis model which represents the hysteresis between martensite fraction and temperature. The structure of the proposed differential hysteresis model is derived from [20] and it constitutes part *II* of Fig. 4.

The $R_m - T$ hysteresis model is given by

$$\begin{cases} \frac{dR_m}{dT} = \begin{cases} \frac{h_-(T)+R_m-1}{h_+(T)-h_-(T)}\, g_+(T), & \dot{T} \geq 0, \\ \frac{h_+(T)+R_m-1}{h_-(T)-h_+(T)}\, g_-(T), & \dot{T} < 0, \end{cases} \\ R_m(0) = 1, \end{cases} \qquad (4)$$

where $g_{+/-}$ and $h_{+/-}$ are given by (5) and (6), respectively.

$$g_{+/-}(u) = \frac{1}{\sigma_{+/-}\sqrt{2\pi}} \exp\left(-\frac{(u-\mu_{+/-})^2}{2\sigma_{+/-}^2}\right), \qquad (5)$$

$$h_{+/-}(u) = \frac{1}{2}\left[1 + \operatorname{erf}\left(\frac{u-\mu_{+/-}}{\sigma_{+/-}\sqrt{2}}\right)\right], \qquad (6)$$

where subscripts $+$ and $-$ denote increasing and decreasing curves, respectively, μ is the mean, and σ^2 is the variance. Note that μ and σ^2 do not have any physical significance. They are simply parameters which govern the shape of the hysteresis loops.

Some favorable properties of the proposed differential hysteresis model are stated and proved in [22].

C. Strain

Suppose that σ_0 is the pretension stress on the SMA wire due to the bias spring, E_a is the elasticity of austenite, k is the bias spring constant, and Δ is the spring deformation in 100% austenite state, ϵ_0 is the strain due to pretension, E_m is the elasticity of fully twinned martensite, E_T is the elasticity of partly twinned martensite, E_d is the elasticity of detwinned martensite, ϵ_m^y is the yield strain of twinned martensite, and ϵ_m^d is the minimum strain of detwinned martensite. Then, the total strain $\epsilon = \epsilon_0 + \epsilon_r$ is given by

$$\epsilon = \begin{cases} \epsilon_0 - \frac{d_1}{2c_1} - \frac{\sqrt{d_1^2 - 4c_1 e_1}}{2c_1}, & \text{if} \quad 0 \leq \epsilon < \epsilon_m^y, \\ \epsilon_0 - \frac{d_2}{2c_2} - \frac{\sqrt{d_2^2 - 4c_2 e_2}}{2c_2}, & \text{if} \quad \epsilon_m^y \leq \epsilon < \epsilon_m^d, \\ \epsilon_0 - \frac{d_3}{2c_3} - \frac{\sqrt{d_3^2 - 4c_3 e_3}}{2c_3}, & \text{if} \quad \epsilon_m^d \leq \epsilon, \end{cases}$$

where c_i, d_i and e_i $(i = 1, 2, 3)$ are functions of R_m, expressions for which are given in the Appendix. For the simulations in this paper, the above expression can be approximated to a polynomial in R_m in order to obtain a continuously differentiable expression for ϵ:

$$\epsilon = \epsilon_0 + k_1 R_m + k_2 R_m^2 + k_3 R_m^{50}, \qquad (7)$$

where k_1, k_2 and k_3 are constant parameters.

This constitutes part *III* of the proposed system model.

D. Electrical Resistance

The SMA wire electrical resistance R is given by

$$\frac{1}{R} = \frac{\pi d_0^2}{4L_0(1+2\epsilon)} \left[\frac{1-R_m}{\rho_a(T)} + \frac{R_m}{\rho_m(T)}\right], \qquad (8)$$

where $\rho_a(T)$ is the electrical resistivity of austenite, and $\rho_m(T)$ is the electrical resistivity of martensite. We propose the following nonlinear expressions for the resistivities, which were found to satisfy experimental results:

$$\rho_a(T) = p_1 + p_2 \exp\left(-p_3(T - T_{amb})\right), \qquad (9)$$

$$\rho_m(T) = (q_1 - q_2 T)\left[1 + \operatorname{erf}\left(\frac{T-m_3}{n_3}\right)\right] + \sum_{i=0}^{i=9} \alpha_i (T - T_{amb})^i, \qquad (10)$$

where p_1, p_2, p_3, q_1, q_2, m_3, n_3 and $\alpha_i (i = 0, ..., 9)$ are constant parameters. This forms part *IV* of the proposed SMA model.

The modules presented in sections II-A, II-B, II-C and II-D, together, constitute the complete differential model of the SMA actuator. Detailed explanation, parameter identification, and simulation results for the model are available in [21]. The next section discusses tracking control of the SMA actuator based on inverse compensation.

III. Tracking Control with Feedback and Inverse Compensation

It was mentioned in Section I that the motivation behind modeling of SMA wire actuator is to be able to control the transformation strain ϵ_r to follow a desired transformation strain trajectory $\epsilon_{rd}(t)$. In [22], a PD tracking controller was applied to the SMA differential model. In this section, we also apply a PID tracking controller. However, since the SMA actuator is highly nonlinear, it is advantageous to implement a nonlinear model-based controller. In this section, we show that the SMA model presented in the previous section is invertible. Using this property, we propose a tracking controller which uses PD feedback with model-based inverse compensation. Simulation results in the next section demonstrate the marked improvement in tracking control accuracy that this controller exhibits over PD and PID controllers.

Fig. 5 illustrates the basic principle behind inverse compensation of SMA actuator. Let the dynamic model of the SMA actuator be denoted by $\epsilon_r = N(vi)$. We compute the inverse compensator $vi = NI(\epsilon_{rd})$. If the inverse is exact, we have

$$\epsilon_r = N(NI(\epsilon_{rd})) = \epsilon_{rd}\,.$$

This is also called feedforward control because the effect of hysteresis and other nonlinearities is compensated (via the inverse model) even before they are encountered. A schematic diagram of the proposed tracking controller is shown in Fig. 6. The saturation block denotes the power bounds on the SMA actuator. For the simulations in this work, $vi \in [0, 4]$ VA.

Similar to the structure of the forward model, the inverse model is derived in a modular fashion. Let the desired transformation strain trajectory be $\epsilon_{rd}(t), \dot{\epsilon}_{rd}(t)$. The strain equation (7) can be written as

$$k_1 R_m(t) + k_2 R_m^2(t) + k_3 R_m^{50}(t) = \epsilon_{rd}(t), \qquad (11)$$

which can be solved for the desired martensite fraction $R_m(t)$. Similarly, $\dot{R}_m(t)$ can also be calculated.

Next, the hysteresis differential equation (4) is inverted. From (4), we write the hysteresis inverse model as

$$\begin{cases} \frac{dT}{dR_m} = \begin{cases} \frac{h_+(T)-h_-(T)}{h_-(T)+R_m-1} \cdot \frac{1}{g_+(T)}, & \dot{R}_m < 0, \\ \frac{h_-(T)-h_+(T)}{h_+(T)+R_m-1} \cdot \frac{1}{g_-(T)}, & \dot{R}_m \geq 0, \end{cases} \\ T(0) = \quad T_{amb}\,. \end{cases}$$

However, the quantities $h_-(T)+R_m-1$, $h_+(T)+R_m-1$, and $g_{+/-}(T)$ can be zero. To prevent the right hand side of the differential equation from blowing up, we modify the

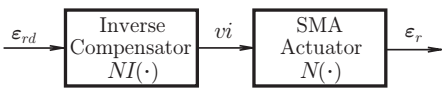

Fig. 5. Schematic block diagram for inverse compensation of SMA actuator

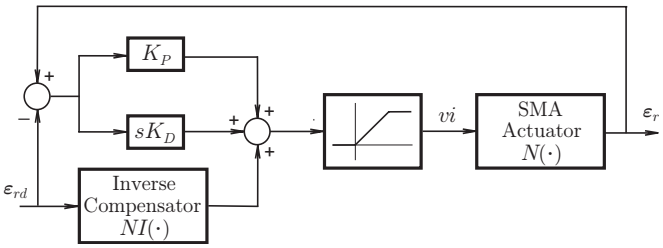

Fig. 6. PD Feedback control with inverse compensation

hysteresis inverse model to obtain

$$\begin{aligned} \frac{dT}{dR_m} &= \begin{cases} \frac{h_+(T)-h_-(T)}{h_-(T)+R_m-1+\delta} \cdot \frac{1}{g_+(T)+\delta}, & \dot{R}_m < 0, \\ \frac{h_-(T)-h_+(T)}{h_+(T)+R_m-1-\delta} \cdot \frac{1}{g_-(T)+\delta}, & \dot{R}_m \geq 0, \end{cases} \\ T(0) &= \quad T_{amb}\,, \end{aligned} \qquad (12)$$

where $\delta > 0$ is an arbitrarily small constant. The desired temperature profile $T(t), \dot{T}(t)$ is obtained by solving (12). Note that (12) is not the exact inverse of (4), which contributes to controller inaccuracy.

Subsequently, the heat transfer equation (1) is written as

$$vi(t) = \rho c \frac{\pi d_0^2 L_0}{4} \frac{dT}{dt} + \pi d_0 L_0 h (T(t) - T_{amb}). \qquad (13)$$

h and c are functions of T and $\dot{T}$. Hence, (13) can be solved for the desired input power $vi(t)$.

Further, the desired input voltage profile $v(t)$ can be calculated, given the power $vi(t)$. This is accomplished using Ohm's law ($v(t) = i(t)R(t)$), by calculating the electrical resistance $R(t)$:

$$\frac{1}{R(t)} = \frac{\pi d_0^2}{4L_0(1 + 2\epsilon_0 + 2\epsilon_{rd}(t))} \left[\frac{1 - R_m(t)}{\rho_a(T)} + \frac{R_m(t)}{\rho_m(T)} \right]. \qquad (14)$$

Equations (11)–(14) constitute the SMA actuator inverse model. Fig. 7 shows the simulink block diagram of the proposed inverse compensation tracking control system.

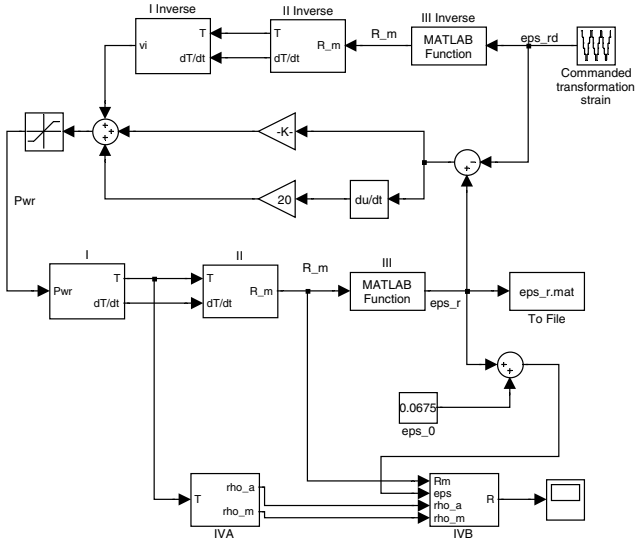

Fig. 7. Simulink block diagram of proposed controller

The next section presents simulation results for the above controller, and their comparison to those for PID controller.

IV. Results

Fig. 8 shows simulation result for tracking along a sinusoidal strain trajectory. At local minima, the commanded trajectory requires a rate of cooling that is higher than that of natural convection. Hence, the actual trajectory lags behind the commanded trajectory. Similarly, the actual transformation strain undershoots the commanded transformation strain as local maxima are approached. Fig. 9 shows the corresponding simulation result for PID controller.

Fig. 10 shows simulation result for tracking along a sawtooth strain trajectory. The small discrepancy between the commanded and the actual trajectory at local minima is explained by the same argument given above. Fig. 11 shows the corresponding simulation result for PID controller.

The above simulation results demonstrate the effectiveness of the inverse controller. We have also shown that the small discrepancies between the commanded and actual trajectories are a result of the physical limitations of the SMA actuator itself, and are not indicative of any drawback in the proposed controller. A comparison of the simulation results for the proposed controller with PD [22] and PID controllers shows that the proposed controller enhances tracking performance. It combines salient features of both PD feedback control and inverse compensation.

V. Conclusions

In this paper, we presented a complete mathematical model for a spring-biased shape memory alloy wire actuator. Based on this model, we proposed a tracking control scheme which consists of an inverse compensator as well as a PD feedback controller.

A salient feature of the proposed model is that it is built around a differential hysteresis model, which uses only four parameters to generate major and minor loops for any arbitrary temperature profile. This presents a significant advantage over algebraic hysteresis models such as [10], [13], as well as Preisach models. Moreover, the differential hysteresis model enables the formulation of state space models of the actuator, and allows for the use of theory of ordinary differential equations for analysis. Further, we showed that the differential hysteresis model is invertible.

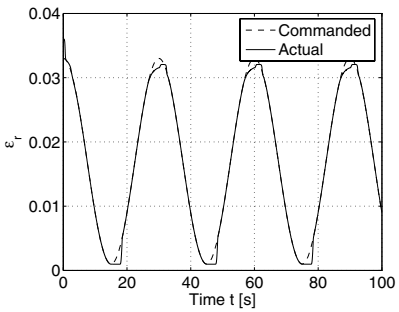

Fig. 8. Proposed controller: sinusoidal commanded transformation strain.

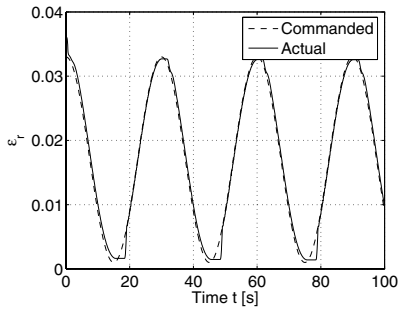

Fig. 9. PID controller: sinusoidal commanded transformation strain.

This facilitated the computation of the inverse model, which forms the basis of the inverse compensation controller for the actuator. Simulation results suggest that the proposed controller achieves higher tracking accuracy than traditional PD and PID controllers. The invertibility property of the SMA model, and the hysteresis model in particular, also makes it applicable to adaptive control applications.

It has been observed that SMAs are highly nonlinear devices which involve complex physics. This behavior makes their modeling and control problematic. Several physics-based thermomechanical models of SMAs (for example [17], [18]) have been proposed, but have not been very useful in control and engineering problems due to their inherent complexities. The model presented in this paper is shown to be mathematically simple, yet effective. Furthermore, control simulations demonstrate the efficacy of the proposed inverse model-based control scheme with feedback.

Acknowledgment

The authors would like to acknowledge the help of Dr. G. Song and his graduate student N. Ma at the University of Houston for making experimental data available for this modeling study.

Appendix

The parametric variables in (II-C) are given by

$$
\begin{aligned}
c_1 &= \pi d_0^2[E_a + (E_m - E_a)R_m], \\
d_1 &= -4kL_0 - \pi d_0^2[E_a + (E_m - E_a)R_m](1 - 2\epsilon_0), \\
e_1 &= 4k\Delta - \pi d_0^2[E_a + (E_m - E_a)R_m]\epsilon_0(1 - \epsilon_0), \\
c_2 &= \pi d_0^2[E_a + (E_T - E_a)R_m],
\end{aligned}
$$

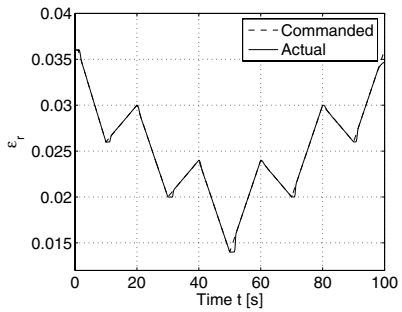

Fig. 10. Proposed controller: sawtooth commanded transformation strain.

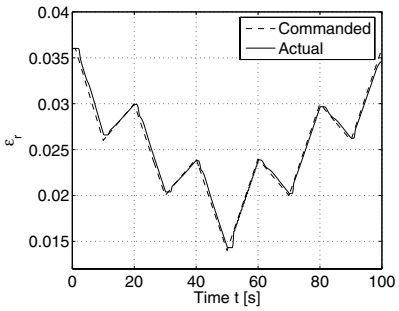

Fig. 11. PID controller: sawtooth commanded transformation strain.

$$
\begin{aligned}
d_2 &= -4kL_0 - \pi d_0^2[E_a + (E_T - E_a)R_m](1 - 2\epsilon_0) \\
&\quad + \pi d_0^2 R_m \epsilon_m^y (E_m - E_T), \\
e_2 &= 4k\Delta - \pi d_0^2(1 - \epsilon_0)[E_a\epsilon_0 + (E_T - E_a)R_m\epsilon_0 \\
&\quad + (E_m - E_T)R_m\epsilon_m^y, \\
c_3 &= \pi d_0^2[E_a + (E_d - E_a)R_m, \\
d_3 &= -4kL_0 - \pi d_0^2[E_a + (E_d - E_a)R_m](1 - 2\epsilon_0) \\
&\quad + \pi d_0^2 R_m[(E_m - E_T)\epsilon_m^y + (E_T - E_d)\epsilon_m^d], \\
e_3 &= 4k\Delta - \pi d_0^2(1 - \epsilon_0)[E_a\epsilon_0 + (E_d - E_a)R_m\epsilon_0 \\
&\quad + (E_m - E_T)R_m\epsilon_m^y + (E_T - E_d)R_m\epsilon_m^d].
\end{aligned}
$$

TABLE I

SIMULATION PARAMETERS

ρ	6500 kgm^{-3}	T_{amb}	24 °C
L_0	0.2286 m	d_0	3.81×10^{-4} m
a_1	165 Wm^{-2}°C^{-1}	b_1	1400 Jkg^{-1}°C^{-1}
a_2	0.5 Wm^{-2}°C^{-2}	b_2	1000 Jkg^{-1}°C^{-1}
a_3	300 Wm^{-2}°C^{-1}	m_1	48 °C
a_4	150 Wm^{-2}°C^{-1}	m_2	58 °C
n_1	10 °C	n_2	0.5 °C
μ_+	78.9 °C	σ_+	11.2 °C
μ_-	34 °C	σ_-	5.8 °C
Δ	0.04425 m	k	58.19 Nm^{-1}
E_a	35917 MPa	E_m	20480 MPa
E_T	826 MPa	E_d	16800 MPa
ϵ_m^y	0.1	ϵ_m^d	0.15
k_1	0.0204	k_2	0.01293
k_3	0.0027		
p_1	9.2×10^{-7} Ωm	q_1	3.4×10^{-8} Ωm
p_2	8.4×10^{-7} Ωm	q_2	5.7×10^{-10} Ωm°C^{-1}
p_3	0.2499 °C^{-1}	m_3	70 °C
n_3	3 °C		
α_0	8.7×10^{-7} Ωm	α_1	4.8×10^{-8} Ωm°C^{-1}
α_2	-7.8×10^{-9} Ωm°C^{-2}	α_3	7.0×10^{-10} Ωm°C^{-3}
α_4	-3.7×10^{-11} Ωm°C^{-4}	α_5	1.2×10^{-12} Ωm°C^{-5}
α_6	-2.5×10^{-14} Ωm°C^{-6}	α_7	3.2×10^{-16} Ωm°C^{-7}
α_8	-2.2×10^{-18} Ωm°C^{-8}	α_9	6.7×10^{-21} Ωm°C^{-9}
k_p	2000	k_d	20
δ	10^{-6}		

REFERENCES

[1] J. Kudva, B. Sanders, J. Pinkerton-Florance, and E. Garcia, "Overview of the DARPA/AFRL/NASA Smart Wing Phase 2 Program," in *SPIE - The International Society for Optical Engineering, Smart Structures and Materials 2001: Industrial and Commercial Applications of Smart Structures Technologies*, vol. 4332, 2001, pp. 383–389.

[2] M. Hashimoto, M. Takeda, H. Sagawa, I. Chiba, and K. Sat, "Shape Memory Alloy and Robotic Actuators," *Journal of Robotic Systems*, vol. 2, no. 1, pp. 3–25, 1985.

[3] K.-Y. Tu, T.-T. Lee, C.-H. Wang, and C.-A. Chang, "Design of a Fuzzy Walking Pattern (FWP) for a Shape Memory Alloy (SMA) Biped Robot," *Robotica*, vol. 17, no. 4, pp. 373–382, 1999.

[4] K. Ikuta, M. Tsukamoto, and S. Hirose, "Shape Memory Alloy Servo Actuator System with Electric Resistance Feedback and Application for Active Endoscope," in *IEEE International Conference on Robotics and Automation*, vol. 1, 1988, pp. 427–430.

[5] M. Bergamasco, F. Salsedo, and P. Dario, "Shape Memory Alloy Micromotors for Direct-Drive Actuation of Dexterous Artificial Hands," *Sensors and Actuators*, vol. 17, no. 1, pp. 115–119, 1989.

[6] K. Gabriel, W. Trimmer, and J. Walker, "A Micro Rotary Actuator using Shape Memory Alloys," *Sensors and Actuators*, vol. 15, no. 1, pp. 95–102, 1988.

[7] R. Jebens, F. Salsedo, and P. Dario, "Microactuators for Aligning Optical Fibers," *Sensors and Actuators*, vol. 20, no. 1, pp. 65–73, 1989.

[8] J. Harrison and D. Hodgson, "Use of TiNi in Mechanical and Electrical Connectors," in *International Symposium on Shape Memory Effects and Applications*, 1975, pp. 517–523.

[9] V. Michaud, "Can Shape Memory Alloy Composites be Smart?" *Scripta Materialia*, vol. 50, no. 2, pp. 249–253, 2004.

[10] K. Ikuta, M. Tsukamoto, and S. Hirose, "Mathematical Model and Experimental Verification of Shape Memory Alloy for Designing Micro Actuator," in *IEEE Micro Electro Mechanical Systems*, 1991, pp. 103–108.

[11] N. Ma, G. Song, and H.-J. Lee, "Position Control of Shape Memory Alloy Actuators with Internal Electrical Resistance Feedback," in *SPIE - The International Society for Optical Engineering, Smart Structures and Materials: Modeling, Signal Processing, and Control*, vol. 5049, 2003, pp. 46–55.

[12] X. Wu, J. Wu, and Z. Wang, "The Variation of Electrical Resistance of Near Stoichiometric NiTi during Thermo-Mechanic Procedures," *Smart Materials and Structures*, vol. 8, pp. 574–578, 1999.

[13] D. Madill and D. Wang, "Modeling and L2-Stability of a Shape Memory Alloy Position Control System," *IEEE Transactions on Control Systems Technology*, vol. 6, no. 4, pp. 473–481, 1998.

[14] V. Brailovski, F. Trochu, and G. Daigneault, "Temporal Characteristics of Shape Memory Linear Actuators and their Application to Circuit Breakers," *Materials and Design*, vol. 17, no. 3, pp. 151–158, 1996.

[15] S. Sukhatme, *A Textbook on Heat Transfer*. Hyderabad: Universities Press, 1996.

[16] J. McNichols and J. Cory, "Thermodynamics of Nitinol," *Journal of Applied Physics*, vol. 61, no. 3, pp. 972–984, 1987.

[17] Z. Bo and D. Lagoudas, "Thermomechanical Modeling of Polycrystalline SMAs under Cyclic Loading, Part IV: Modeling of Minor Hysteresis Loops," *International Journal of Engineering Science*, vol. 37, pp. 1205–1249, 1999.

[18] A. Bekker and L. Brinson, "Phase Diagram based Description of the Hysteresis Behavior of Shape Memory Alloys," *Acta Materialia*, vol. 46, no. 10, pp. 3649–3665, 1998.

[19] Y. Ivshin and T. Pence, "A Constitutive Model for Hysteretic Phase Transition Behavior," *International Journal of Engineering Science*, vol. 32, no. 4, pp. 681–704, 1994.

[20] A. Likhachev, "Differential Equation of Hysteresis: Application to Partial Martensitic Transformation in Shape-Memory Alloys," *Scripta Metallurgica et Materialia*, vol. 32, no. 4, pp. 633–636, 1995.

[21] S. Dutta and F. Ghorbel, "Differential Hysteresis Modeling of a Shape Memory Alloy Wire Actuator," *IEEE/ASME Transactions on Mechatronics*, vol. 10, no. 2, April 2005, to appear.

[22] S. Dutta, F. Ghorbel, and J. Dabney, "Dynamic Modeling and Control of Hysteresis in a Shape Memory Alloy Actuator," in *International Mechanical Engineering Congress and RD&D Expo*. Anaheim, CA: ASME, November 2004.